

# Quantum Cellular Automata for the Analysis of Entanglement Complexity in Quantum Many-Body Systems

Patrick Rall - Undergraduate Junior in Physics, Caltech Class of 2016  
Advised by Nicole Yunger Halpern and Ning Bao, John Preskill Theory Group  
Institute for Quantum Information and Matter, Caltech

## Abstract

Quantum information science often benefits from quantum extensions of classical game theory. Cellular automata are one-player games used in classical studies to generate complexity. Quantum cellular automata can be similarly used to study the complexity of quantum many-body systems. Since classical block cellular automata like Critters are defined by a local unitary operation they can easily be generalized using quantum circuits. A two or three-qubit quantum circuit is extended to a time evolution acting on an entire  $N$ -qubit grid. Many quantum block cellular automata can be simulated exactly using a matrix product state despite exhibiting exotic entanglement structure, hence providing a testbed for measures of entanglement complexity. In this analysis we investigate networks formed by measures on two-qubit subsystems including mutual-information, negativity and quantum concurrence. Additionally, generated states are compared to real-world systems in terms of area laws and correlation-length decay.

## Introduction

The Game of Life is a cellular automaton developed by the British mathematician John Conway. Featuring a 2D grid of cells that can be either ‘dead’ or ‘alive’ and rules governing the evolution of the cells’ states, this simple system evolves complex, sometimes chaotic behaviors that model real-life processes. By extending this model to permit quantum superpositions of ‘dead’ and ‘alive’ cells, we can explore entanglement complexity in quantum many-body systems with. The resulting time evolution is not necessarily based on real-life Hamiltonians, but instead is geared to produce states exhibiting particular kinds of entanglement complexity.

There are at least four<sup>1</sup> methods for quantizing cellular automata, each with advantages and disadvantages. One approach studied in [1] encodes the update rule of Conway’s Game of Life—changing a cell’s state based on the number of alive neighbors—into a Hamiltonian reminiscent of some condensed-matter systems. This analogy creates a reversible quantum update rule inspired by an irreversible classical rule. A consequence of this approach is that the quantum version behaves very differently from the original. This issue is also present for quantizations of elementary cellular automata [3], such as rule 110, which are largely irreversible. The only reversible rules consist of trivial behavior, e.g., flipping

---

<sup>1</sup>Some examples are a Hamiltonian version of Conway’s Game of Life [1], the quantum block cellular automata discussed in this article, as well as quantum elementary cellular automata and quantum reversible elementary cellular automata to be discussed in future work. Elementary cellular automata are discussed in [3].

a cell's state or shifting the board one bit to the left.

As Norman Margolus argues in [2], an irreversible rule can cause the system to evolve from a complex initial configuration to a short-period cycle. If a cellular automaton (CA) has a reversible update rule, the only way it can cycle is by reaching its initial state. This causes the average cycle period to be significantly longer because the CA must explore a larger fraction of its state space before a cycle can start again. So, since reversibility appears to have a significant effect on the CA's emergent properties, constructing a reversible quantum CA from a classical irreversible CA may result in the quantum being incomparable to the classical CA.

To avoid this, I shall focus on block CA discussed in [2]. Their update method involves partitioning the board into small pieces of equal size and shape, then applying a reversible transform to these pieces. This process is repeated over several possible partitionings of the board, resulting in non-trivial but reversible evolution. The 'Critters' rule is a block CA which is known to replicate many interesting emergent properties of Conway's Game of Life. The classical rule can be generalized to a quantum rule, as reversible permutations of each block's state space can be represented via by unitary operators. Classical permutations of state can be extended via quantum gates, such as the Hadamard gate. This would allow the CA to introduce new superposition and entanglement. The nature of these quantum properties is more predictable for block CAs than for CAs based on a Hamiltonian. This is because extrapolating the unitary classical transformation to a quantum time evolution

preserves reversibility.

## Methods

### Rule formalism

Consider a one dimensional  $N$ -qubit system that begins in the state  $|\Psi\rangle$ . Let  $U_k$  denote a unitary defined on a subsystem of  $k$  qubits. Such a  $U_k$  is called an *update rule*. From  $U_k$ , we can construct  $k$  unitaries  $\mathbb{U}_i$  defined on the  $N$ -qubit system where  $i \in \{0, \dots, k-1\}$ . An iteration of the CA consists of transforming a state  $|\Psi\rangle$  to  $\mathbb{U}_{k-1}\dots\mathbb{U}_0|\Psi\rangle$ .

$\mathbb{U}_i$  is constructed by applying  $U_k$  to adjacent  $k$ -qubit subspaces, such that all  $N$ -qubits are acted upon by some  $U_k$  except for some at the edges of the board. The  $i$  in  $\mathbb{U}_i$  denotes the number of qubits on the left side of the board not acted on by any  $U_k$ . The first  $U_k$  is applied to the  $(i+1)$ 'th to  $(i+k)$ 'th qubits, the second to the  $(i+k+1)$ 'th to  $(i+2k)$ 'th, and so on. This process is repeated across the board until less than  $k$  qubits are left.  $\mathbb{U}_i$  can be written in terms of  $U_k$  and the  $j$ -qubit identity gate  $\mathbb{I}_j$ :

$$\mathbb{U}_i = \mathbb{I}_i \otimes U_k \otimes \dots \otimes U_k \otimes \mathbb{I}_{N-i-k[(N-i) \bmod k]}.$$

Since there are  $[(N-i) \bmod k]$  instances of the  $U_k$  operator, any  $\mathbb{U}_i$  acts on an  $i+k[(N-i) \bmod k] + (N-i-k[(N-i) \bmod k]) = N$ -qubit system. The full iteration of the CA is an application of all possible  $\mathbb{U}_i$ , i.e., all different possible positions of the  $U_k$  operator tiled across the board (see Figure 1). This definition is the 1D version of 2D block CAs like the 'Critters' rule.

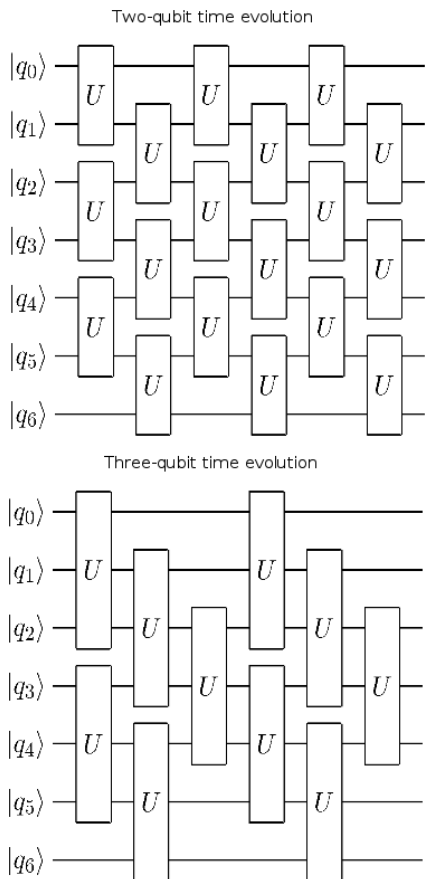


Figure 1: Quantum circuits showing time evolution of block CAs generated by two-qubit or three-qubit gates  $U$  for a system with seven sites. Time progresses from left to right in the diagram. Without periodic boundary conditions, some edge qubits must be left unchanged at every step.

Classical block CAs consist of operators  $U_k$  defined by a permutation of  $k$ -bit states. Since a matrix representing a permutation is unitary, such a  $U_k$  represents the time evolution of not just a classical system but also a closed quantum system. If  $U_k$  is a permutation then the above update method replicates classical behaviors if the initial state

is neither entangled nor a nontrivial superposition. By augmenting  $U_k$  with quantum gates like the Hadamard gate, iterations of the CA can introduce new superposition and entanglement.

Since there are  $2^k$  configurations of  $k$ -bit states, there are  $2^k!$  possible classical permutations. This gives 24 two-bit rules and 40320 three-bit rules. Due to the size of the classical portion of the rule space,  $k \in \{2, 3\}$  provides a sufficient number of rules for this analysis.

### Complex networks

The Quantum Cellular Automata (QCAs) above are simulated using a Matrix Product State (MPS) in canonical form. MPS with open boundary conditions allows constant-time extraction of any single-qubit density matrix and time evolution of the state polynomial in  $N$ . These efficiencies are retained provided the Schmidt-number  $\chi$  remains bounded by a constant [4]. States with relatively low entanglement complexity have low  $\chi$ . This permits simulation and visualization of a QCA inside a web-browser with system size  $N < 60$  and  $\chi < 10$ . Furthermore, the MPS describes the amount of entanglement between the left half and the right half of a system split at any point.

While this information is useful for understanding the entanglement of simple superpositions like Bell pairs, it is insufficient for more complex behavior. A better characterization of states with more complex entanglement can be achieved via a network of two-qubit measures of correlation and entanglement. Each vertex in the network represents a qubit and each edge connecting two vertexes is weighted by the value of

the measure on the corresponding two-qubit subsystem. In other words, the network’s adjacency-matrix elements  $A_{ij}$  are given by the measure on qubits  $i$  and  $j$ . All 2-qubit density matrices  $\rho_{ij}$  can be extracted from a MPS in  $N^2$  time.

One useful quantity is the mutual-information

$$\mathcal{I}_{ij} = \frac{1}{2}(S_i + S_j - S_{ij}),$$

defined in terms of the von Neumann entropy  $S_{ij} = -\text{Tr}(\rho_{ij} \log \rho_{ij})$ . Here  $\rho_{ij} = \text{Tr}_{\text{all qubits but } i,j}(|\Psi\rangle\langle\Psi|)$ , where  $|\Psi\rangle$  is the state of the whole system. While containing classical correlations as well as quantum correlations,  $\mathcal{I}_{ij}$  upper-bounds entanglement measures, which is one reason  $\mathcal{I}_{ij}$  was chosen for complex network measures in [7].

An entanglement monotone that captures quantum correlation only is the negativity

$$\mathcal{N}_{ij} = \frac{1}{2}(\text{Tr}|\rho_{ij}^{T_i}| - 1),$$

based on the positive-partial-transpose criterion for separability [10, 11]. Here  $\rho_{ij}^{T_i}$  represents the reduced density matrix of qubits  $i, j$  with the  $i$ ’th qubit’s sub-matrix transposed.

Quantum concurrence is an entanglement measure defined by

$$\mathcal{C}_{ij} = \max(0, \lambda_1 - \lambda_2 - \lambda_3 - \lambda_4)$$

. Here  $\lambda_i$  are the eigenvalues, in decreasing order, of the matrix  $\rho_{ij}(\sigma_y \otimes \sigma_y)\rho_{ij}^*(\sigma_y \otimes \sigma_y)$  where  $\sigma_y$  is a Pauli matrix [12].

Each of these measures achieve different characterizations of two-qubit correlation and entanglement, e.g., concurrence exhibits monogamy of entanglement. To provide intuitions about how these measures

compare, their networks will be calculated for states generated by QCAs.

## State visualization

Visualization is the most common method for assessing the output of classical CAs. A visualization of quantum many-body systems in the computational basis is essential for a quantum analogy. Classical cell colors are commonly represented by two colors: black and white. In the quantum case this binary set of possibilities must be extended to represent a single-qubit density matrix. This is achieved by mapping the surface of the Bloch sphere to colors as shown in Figure 2. Position is given by  $\vec{r}$  defined by

$$\rho = \frac{I + \vec{\sigma} \cdot \vec{r}}{2}.$$

Here,  $\rho$  is the single-qubit reduced density matrix and  $\vec{\sigma}$  is the vector of Pauli matrices.

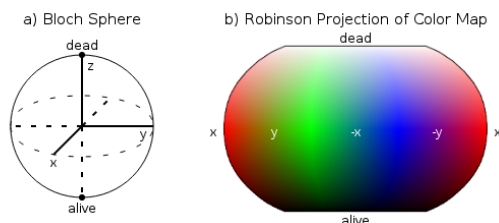


Figure 2: Robinson projection of a Bloch sphere representing the assignment of each qubit pure state to a color. For a pure state given by  $|\psi\rangle = \sin(\theta/2)|\text{alive}\rangle + \cos(\theta/2)e^{i\phi}|\text{dead}\rangle$ , phase  $\phi$  is mapped to a cycle over the colors red, green, and blue. The angle  $\theta$  maps to the overall brightness.

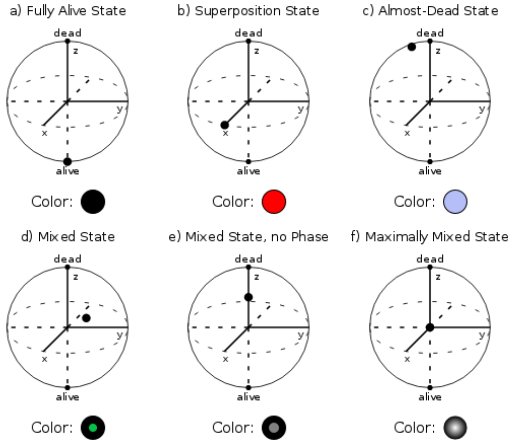


Figure 3: Some examples of single-qubit density matrices, showing their representations as points inside the Bloch sphere and the color of the corresponding cells. Direction of the Bloch vector  $\vec{r}$  gives the color, and the degree of mixedness  $1 - |\vec{r}|$  gives the border thickness.

Since  $|\vec{r}| \leq 1$ ,  $\vec{r}$  represents a position on the surface of or inside the Bloch sphere. States on the surface of the sphere are pure states, while states inside the sphere are mixed states. To achieve a complete representation of  $\rho$  in a cell, cell color is taken from the direction of  $\vec{r}$  and border thickness is given by  $1 - |\vec{r}|$ . When  $\vec{r} = \vec{0}$ , the qubit is in a maximally mixed state and receives a unique representation featuring a radial gradient. Some examples are given in Figure 3, with the maximally mixed state shown in Figure 3f.

## Discussion

Some particularly interesting quantum circuits are shown in Figure 4. These circuits generate time evolutions exhibiting many of the properties discussed below.

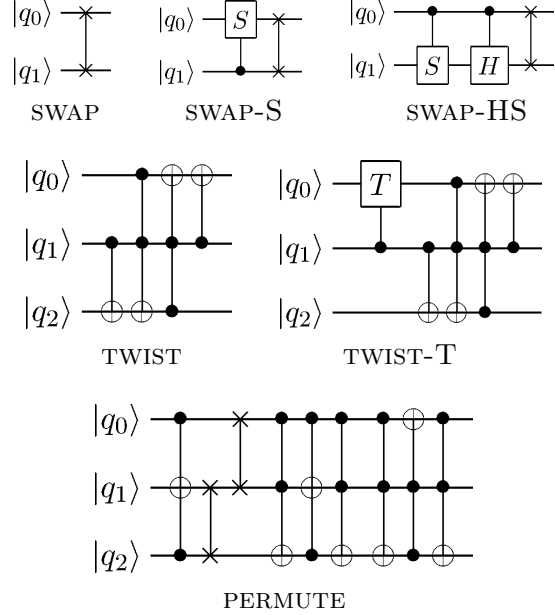


Figure 4: Some examples of quantum circuits generating interesting time evolution when applied as a block CA. SWAP, TWIST and PERMUTE are classical permutations. The variations on these with quantum circuits can change a qubit's phase and generate new superposition.

## Quantum Gliders

A test for whether block QCAs yield complex behavior is to see if emergent properties that make Conway's Game of Life interesting can be replicated. The primary examples are 'gliders': a set of configurations that form a cycle. The sequence of configurations moves by some offset  $s$  with every cycle. These gliders can collide with static structures or other gliders, causing them information to move across the board. If a neighborhood of width  $m$  at position  $i$  is in configuration  $C_{m,i,0}$ , a glider represents a structure that undergoes transitions  $C_{m,i,0} \rightarrow C_{m,i,1} \rightarrow C_{m,i,2} \rightarrow \dots \rightarrow C_{m,i+s,0}$ .

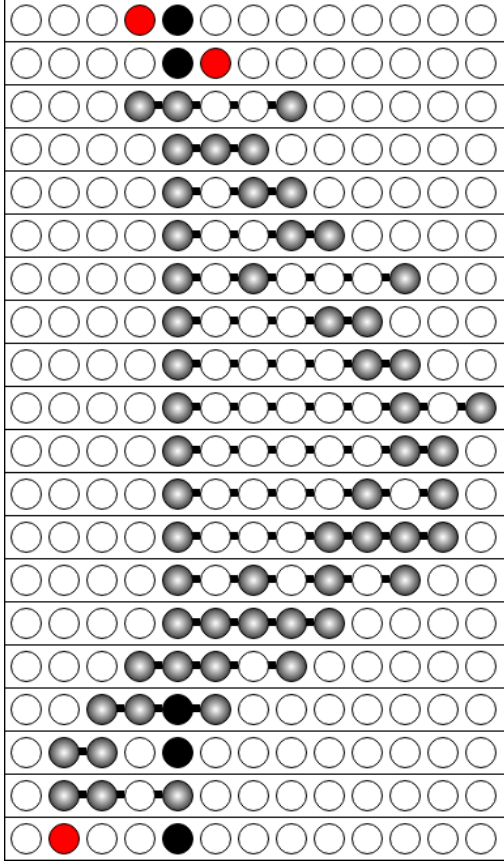


Figure 5: Evolution of PERMUTE, showing a quantum glider. Time flows from top to bottom. Black lines connecting qubits show the von Neumann entropy of the entanglement between the left half and right half of the system. The initial state has a neighborhood at position  $i = 4$  whose configuration is of the form  $(|C_{i,0}\rangle + |C'_i\rangle)/\sqrt{2}$  where  $C_{i,0}$  is a glider and  $C'_i$  is not.  $C_{i,0}$  propagates to the right, bounces off the right edge, and then propagates leftward.  $C'_i$  is left behind and remains at a constant position.

Many block QCAs generate these structures. In the simplest case, SWAP yields gliders that consist of single ‘alive’ excitations that move leftward or rightward, depending

the parity of their initial positions. The gate PERMUTE exhibits a right-moving glider that conserves the number of live qubits, and a left-moving glider that cycles between three and four live qubits.

These gliders can have quantum properties: if a neighborhood is initialized to a state  $(|C_{i,0}\rangle + |C'_i\rangle)/\sqrt{2}$ , where  $C_{i,0}$  is a glider configuration and  $C'_i$  is not, half of the superposition will propagate and the other half will remain stationary. With most rules, including PERMUTE, the qubits in structures are entangled with each other. An example of such a quantum glider is shown in Figure 5.

If an initial state  $(|C_{i,0}\rangle + |C_{i,1}\rangle)/\sqrt{2}$  is prepared, where both configurations are members of the same glider, a structure is formed that is simultaneously in two configurations of a glider cycle. TWIST features such a glider that cycles between product states and entangled states as it moves. Gliders can become entangled with each other after a collision. With SWAP-S single superposed qubits form gliders that undergo a conditional phase rotation during every collision, causing them to entangle.

Rules that consist entirely of classical permutations tend to only produce entanglement with these quantum gliders. However, rules with quantum extensions, such as controlled-Hadamard, generate new superposition and entanglement that can spread across the board via quantum gliders. This results in large-scale patterns with non-trivial entanglement structure. The entanglement behaviors of large-scale patterns are difficult to characterize by mere inspection, unlike the entanglement behaviors of quantum gliders.

## Entanglement Structure

When entanglement structure is simple, as in Figure 5, the von Neumann entropy of entanglement between the system’s left and right halves, along with each qubit’s reduced density matrix is often sufficient for understanding the overall structure. For states with more intricate entanglement structure this information does not provide a satisfying characterization, for instance, in the state shown in Figure 6. Complex networks are a sophisticated tool for characterizing the entanglement structure.



Figure 6: A state of entangled qubits generated by TWIST-T. Individual qubit states are easily visible by their corresponding cells. The entanglement appears homogeneous because the links between cells are about equally dark. Network analysis, though, reveals the entanglement’s structure.

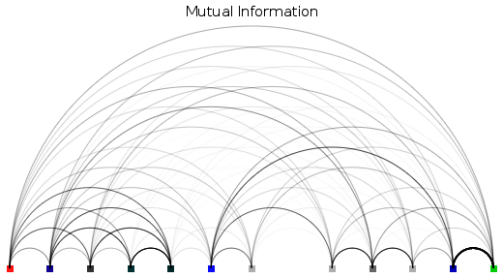


Figure 7: Depiction of a mutual-information network of the state shown in Figure 6. Thicker lines mean larger mutual-information and the squares on the bottom represent the qubits in Figure 6. This representation shows more clearly which qubit is correlated with which other qubit.

Figure 7 is a representation of a mutual-

information network inspired by [7]. Details about the entanglement that were invisible in Figure 6 are now visible. While the entanglement appeared homogeneous in Figure 6, we now observe that the entanglement has non-homogeneous structure. Both short-range entanglement and long-range entanglement are present in this state. The information yielded by  $\mathcal{I}_{ij}$  is rich because classical correlations are measured as well. This has the disadvantage that qubit pairs with high mutual-information are not necessarily entangled—it is merely an upper bound.

We can even make some inferences about the state’s history. Since there exists entanglement between opposite ends of the system, but less entanglement with the edges and the center, we can guess that at some point a quantum glider propagated from one side to the other.

Quantum cell colors fully characterize degrees of freedom local to each qubit. A full characterization of entanglement is difficult to achieve, even with entanglement networks. From examples like the  $N$ -qubit GHZ state  $(|0\dots 0\rangle + |1\dots 1\rangle)/\sqrt{2}$ , we know that three-qubit entanglement can be invisible when only looking at two-qubit subsystems. Hence measures defined on pairs of qubits cannot fully characterize entanglement. Partial descriptions remain useful, however, as complex network measures were shown to be indicators of phase transitions in [7].

Another difficulty is separating classical correlation from quantum correlation, given a two-qubit mixed state. mutual-information captures quantum correlations, but captures some classical correlations as well. Negativity is an entanglement monotone [13] that can only be nonzero if the two-

qubit subsystem is inseparable.

Figure 8 shows that restricting to quantum correlation involves losing a lot of intuition about the entanglement structure. When two-qubit reduced states are extracted from a whole-system state that contains multi-qubit entanglement, some quantum correlations are reduced to residual classical correlations. This shows why mutual-information characterizes the correlations in a richer manner because potential multi-qubit entanglement is visible via residual classical correlations.

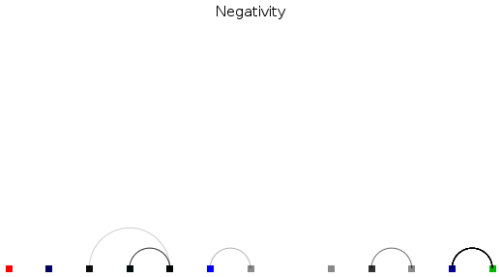


Figure 8: Depiction of a negativity network for the state shown in Figure 6. Despite the many correlations in Figure 7, there appears to be little two-qubit entanglement.

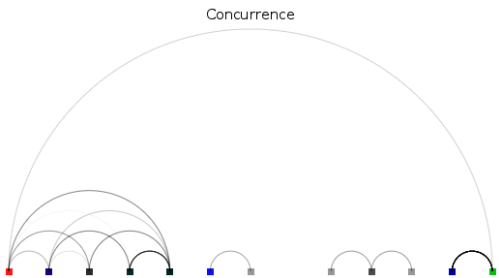


Figure 9: Depiction of a concurrence network for the state shown in Figure 6. This entanglement measure captures more two-qubit entanglement than negativity.

Other entanglement measures like quantum concurrence, exhibit a similar issue: by

measuring only quantum correlations of two-qubit subsystems we fail to get indicators of some kinds of entanglement with more than two qubits. Comparing Figures 8 and 9, we see concurrence captures more two-qubit entanglement than negativity. Structures that were visible in the mutual-information network in Figure 7 are reproduced in Figure 9, such as the group of five entangled bits on the left and the long-range entanglement between qubits on opposite ends of the board.

Gaining intuitions about the relationships between correlation measures is difficult, given just the measures’ definitions. By applying measures to states generated by QCAs we can learn more about their characterization of different types of many-body entanglement. Better intuition about the measures’ properties could guide their application to real-world many-body systems.

### Area Law Analysis and Correlation-Length Decay Analysis

QCAs are not real-world systems, so it is interesting to study how they deviate from reality. This can be approached via analysis tools used to understand condensed-matter systems. Consider the time evolution of the SWAP-HS CA—a combination of a classical rule generating moving particles and the controlled-Hadamard and controlled-phase gates. In Figure 10, a single particle leaves behind a trail of excitations. As the trail bounces across the board, the qubits homogenize. One could compare this behavior to the dropping of a stone into a puddle: over time, the local excitation will cause the entire board to exhibit excitations that look locally similar.

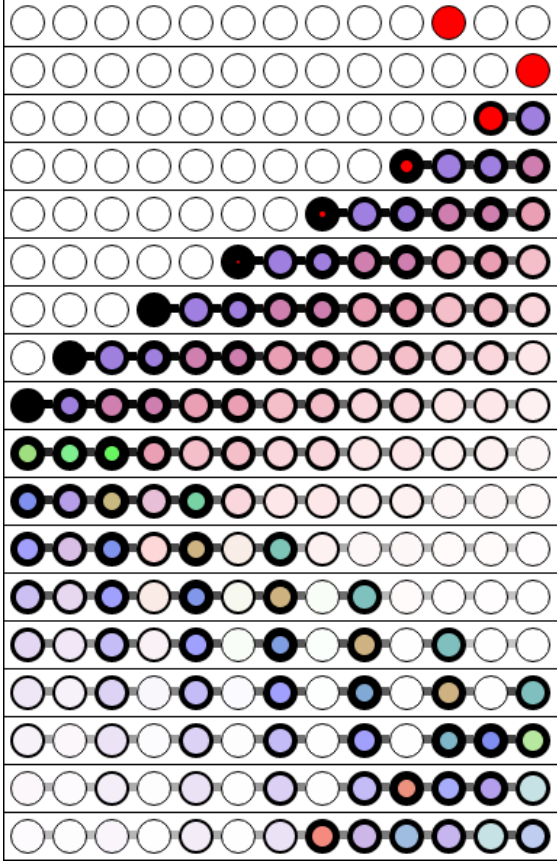


Figure 10: Time evolution of SWAP-HS starting from a single excitation. Time progresses from top to bottom. The CA is a combination of classical permutations which cause particles to move around the board, the controlled-Hadamard gate which generates new excitations, and the controlled-phase gate which causes the phases of the qubits to interact.

Many real physical states obey an area law: the amount of entanglement of a subsystem with its surroundings is proportional to the area of its boundary [4]. This is usually true for states where entanglement is short-range [4]. Contiguous subsystems in a one dimensional system have a constant

boundary size. In a state with an area law the amount of entanglement of subsystem of adjacent qubits, called a subrange, with the rest of the system is independent of its length. Figure 10 shows that for subsystems smaller than  $N/2$  this property is satisfied.

This is on the one hand unsurprising, given the analogy to ripples in a puddle. On the other hand, the entanglement of the final state in Figure 10 is not fully homogenized, so it is perhaps more surprising that an area law is present before the system has fully equilibrated. This could be a consequence of the small system size.

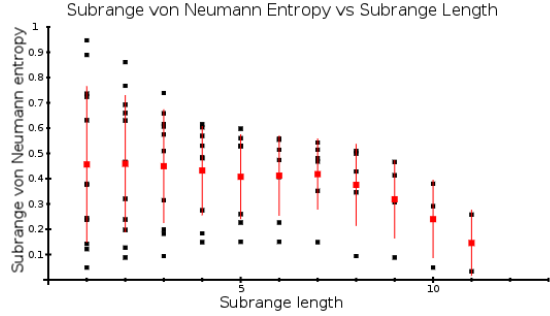


Figure 11: Area-law analysis of the final state shown in Figure 10: the von Neumann entropy of a subrange of qubits with the rest of the system is plotted against the length of the subrange. Neglecting large subranges ( $|i - j| > N/2$ ), we observe that subrange entanglement is a constant function of subrange length. The mean and standard deviation for each separation distance are shown in red.

Correlators such as  $\langle Z_i Z_j \rangle$  defined by operators like the  $Z = \sigma_z$  Pauli matrix acting in sites  $i$  and  $j$  are commonly used in condensed-matter physics because they can be measured in experiments. The variation

of these correlators with the distance between qubits  $i$  and  $j$  can signal phase transitions. Large equilibrium systems usually exhibit exponential decay of correlation unless the system is close to a critical point, in which case polynomial decay is observed [14, Chapter 4]. Figure 12 shows the relation between  $\langle Z_i Z_j \rangle$  and  $|i - j|$  for the final state in Figure 10. Rather than decaying, the correlation remains constant as a function of distance. While this comparison is more meaningful for large systems, the fact that no decay at all is present is still surprising because the state has an area law.

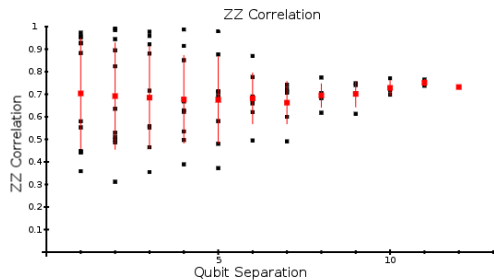


Figure 12: ZZ-correlation-length-decay analysis of the final state shown in Figure 10:  $\langle Z_i Z_j \rangle$  is plotted against  $|i - j|$  for all pairs of qubits. Instead of decaying, the correlation remains constant as a function of distance. The mean and standard deviation for each length are shown in red.

The fact that qubit correlation is constant in their separation distance could result from the final state of Figure 10 not being in equilibrium. However, simulating the evolution further shows that the lack of correlation decay remains even once the system is fully homogenized. The fact that the system already exhibits an area law after the iterations shown in Figure 10 also suggests equilibrium features could be present.

This illustrates that QCAs can violate expectations commonly satisfied by real-world systems. Special states that obey an area law but contain long-range entanglement can be generated. Therefore, QCAs could also serve as a testbed for measures in non-equilibrium quantum statistical physics—for example by comparing to physical systems after a quench.

## Conclusions

Quantum many-body systems have diverse and interesting properties that are often counterintuitive. Understanding the entanglement structure of these systems is essential for condensed-matter physics. Quantum cellular automata are complexity generators that can be engineered to produce states with particular kinds of complexity like quantum gliders. By providing concrete examples of entangled many-body states, they provide a testbed for tools for understanding entanglement complexity.

Complex networks of two-qubit quantities like mutual-information and entanglement measures are examples of tools for understanding many-body entanglement. They are examples of how research in quantum information science can connect with condensed-matter physics. By calculating networks for states generated by quantum cellular automata, detailed information about the structure of the correlations and entanglement can be extracted. A complex network often provides enough information about a state that educated guesses about the state’s history can be made. One can also compare how different two-qubit quantities characterize the structure of en-

tangled states. Collecting information from only two-qubit subsystems results in some loss of entanglement information. Therefore extending complex networks to measures of subsystems with three or more qubits could possibly yield even more powerful tools.

Quantum cellular automata could have many more applications. Applying tools like area law analysis and correlation length can create an analogy to real-world systems. If quantum cellular automata acting on large systems are considered one could study important ideas in condensed-matter physics such as topological order. There also exist quantum cellular automata that can perform universal quantum computation [6]. Thus, finding approximate implementations of quantum cellular automata using real-world Hamiltonians could result in methods for building a quantum computer. With many possible applications, quantum cellular automata are an exciting topic in theoretical physics worthy of more study in the future.

## Acknowledgments

This project would not have been possible without guidance and support from many people. I would like to thank:

- my advisers Nicole Yunger Halpern and Ning Bao for advice throughout the project, guidance with weekly meetings and feedback on my results and writing,
- John Preskill for giving me the opportunity to work in an advanced research group, as well as comments on project directions and useful questions,

- Lincoln Carr, David Vargas and Logan Hillberry at the Colorado School of Mines, as well as Simone Montenegro at the Institute for Quantum Information in Ulm for a great collaboration and insights about different approaches,
- Eugene Mozgunov for many interesting discussions on project directions and suggestions for interesting quantities and analysis tools.

## References

- [1] D. Bleh, T. Calarco, S. Montangero “Quantum Game of Life”, arXiv:1010.4666, 2012
- [2] N. Margolus, “Crystalline Computation”, Chapter 18 of *Feynman and Computation* (A. HEY, ed.), Perseus Books (1999)
- [3] S. Wolfram, “Statistical mechanics of cellular automata” 0.1103/RevModPhys.55.601
- [4] R. Orus. “A Practical Introduction to Tensor Networks: Matrix Product States and Projected Entangled Pair States”
- [5] F. Verstraete, J.I. Cirac, V. Murg “Matrix Product States, Projected Entangled Pair States, and variational renormalization group methods for quantum spin systems” arXiv:0907.2796v1
- [6] R. Raussendorf, “Quantum cellular automaton for universal quantum computation” 10.1103/PhysRevA.72.022301

- [7] D Vargas, L. Carr “Detecting Quantum Phase Transitions via Mutual Information Complex Networks” arXiv:cond-mat.stat-mech/1508.07041
- [8] G. K. Brennen, J. E. Williams, “Entanglement Dynamics in 1D Quantum Cellular Automata” arXiv:quant-ph/0306056v1
- [9] M. Ziman, P. Stelmachovic, V. Buzek, M. Hillery, V. Scarani, N. Gisin ”Quantum Homogenization” arXiv:quant-ph/0110164
- [10] A. Peres, “Separability Criterion for Density Matrices” PhysRevLett.77.1413
- [11] M. Horodecki, P. Horodecki, R. Horodecki, “Separability of mixed states: necessary and sufficient conditions” doi:10.1016/S0375-9601(96)00706-2
- [12] S. Hill, W. Wootters, “Entanglement of a Pair of Quantum Bits” arXiv:quant-ph/9703041
- [13] J. Eisert “Entanglement in quantum information theory” arXiv:quant-ph/0610253
- [14] M. Kardar “Statistical Physics of Fields” ISBN 078-0-521-87341-3